THE JOURNAL OF BIOLOGICAL CHEMISTRY VOL. 280, NO. 40, pp. 34003–34007, October 7, 2005

The Identification of Apoptosis-related Residues in Human Thymosin β-10 by Mutational Analysis and Computational Modeling*

Received for publication, February 11, 2005, and in revised form, July 12, 2005 Published, JBC Papers in Press, July 12, 2005, DOI 10.1074/jbc.M501629200

Seung Bae Rho[‡1], Keun Woo Lee[§1], Taehoon Chun[¶], Seung-Hoon Lee[‡], Kyoungsook Park[‡], and Je-Ho Lee[‡‖2]

From the [‡]Molecular Therapy Research Center, Sungkyunkwan University, Samsung Medical Center Annex 8F, 50 Ilwon-Dong, Kangnam-Ku, Seoul 135-710, Korea, [‖]Division of Gynecologic Oncology, Department of Obstetrics and Gynecology, Samsung Medical Center, Sungkyunkwan University School of Medicine, 50 Ilwon-Dong, Kangnam-Ku, Seoul 135-710, Korea, [§]Division of Applied Life Science, Environmental Biotechnology National Core Research Center, Gyeongsang National University, 900 Gazwa-Dong, Jinju 660-701, Korea, and [¶]Department of Microbiology and Immunology, School of Medicine, Hanyang University, Haeng-dang-Dong, Sung-dong-Ku, Seoul 133-791, Korea

Thymosin β-10 (TB10) is an actin monomer-sequestering peptide that consists of 43 amino acid residues and that tends to form α-helical structures. Previously, we showed that the overexpression of TB10 dramatically increases the frequency of apoptosis in human ovarian cancer cells. To identify the critical residues responsible for TB10-mediated apoptosis, we used a series of computational methods. First, a three-dimensional structure of human TB10 was constructed using the homology modeling method with the calf thymosin β-9 NMR structure as a template. Although the sequences of both of these structures are almost identical, 200-ps molecular dynamics simulation results showed that their secondary structures differ. Analyses of molecular dynamics snapshot structures suggested that the TB10 structure is conformationally more complicated than the TB9 structure. The conserved ^{17}LKKTET^{22} motif region of TB10 was tested by Ala and Ser scanning mutagenesis using computational and biochemical methods, and 12 mutants were transfected into cancer cell lines and tested for their effects on growth arrest. Of the 12 mutants examined, only the Thr^{20} to Ser^{20} mutation showed reduced growth arrest. These results strongly suggest that Thr^{20} is specifically required for actin sequestration by TB10 in ovarian cancer cells. These results may provide useful information for the development of a new ovarian cancer therapy.

The β-thymosins are small (molecular mass < 5 kDa) highly conserved acidic proteins. They were originally identified in calf thymus and thought to be involved in immunomodulatory functions (1). At least 16 β-thymosin isoforms have been identified from various vertebrates and invertebrates, and most, including thymosin β-4 (TB4),[3] are constitutively expressed in most tissues (2–5). A majority share a conserved hexapeptide motif, "LKKTET," which is critical for binding actin, and have important roles in maintaining cellular functions, such as cell morphology, proliferation, and locomotion (6). In most mammalian tissues, TB4 and TB10 are major actin monomer-sequestering proteins (7, 8). Both form a 1:1 complex with G-actin and inhibit its polymerization to F-actin (9–11).

TB10 is more selectively modulated during embryological development than TB4 and is associated with several diseases (12–15). In addition, TB10 up-regulates the anti-apoptotic protein Bcl-2, which is associated with neoplastic transformation (16). Thymosin β-9 (TB9) overexpression was also found to modulate infected bovine macrophage apoptosis (17).

In the present study, we employed a combined approach involving molecular modeling and site-directed mutagenesis to better understand the molecular regions of TB10 that control apoptosis. On the basis of its computer model-determined three-dimensional structure, we identified a region of TB10 that might be critical for apoptotic induction. This region was then tested in transfected ovarian cancer cell lines via mutagenesis (Ala and Ser scanning) of the conserved ^{17}LKKTET^{22} motif with respect to actin binding.

EXPERIMENTAL PROCEDURES

Computer Modeling Study: Three-dimensional Structure Generation, Structure Refinement, and Point Mutations—A three-dimensional structure of a target protein is critically required for computational or molecular modeling studies. Thus, because the three-dimensional structure of TB10 was unavailable from either x-ray or NMR studies, the homology modeling method was employed to build the TB10 three-dimensional structure using the known structure of its TB9 homolog, which was determined by the NMR method for TB9 (Protein Data Bank code: 1HJ0) (18). The sequence identity between these entities is 87.8%. The MODELER module in the INSIGHT II program (Accelrys, Inc., San Diego, CA) was used for the calculation.

After building the three-dimensional structure of TB10, the modeled structure was refined by energy minimization (EM) and MD simulations after surrounding the structure with a 10-Å water layer of 1413 water molecules. The calculations were performed with the DISCOVER module in the INSIGHTII program using the consistent-valence forcefield (20). For the EMs, 500 steps of conjugate gradient scheme were performed with a tolerance of 0.05 kcal/mol. The 20-ps MD runs were used for the system equilibration at 300 K, and these were followed by 200-ps production runs. The integration time step for the MD simulations was 1 fs.

To identify the critical residue in the conserved motif, ^{17}LKKTET^{22}, the six residues were mutated to Ala or Ser using the BIOPOLYMER

* This work was supported by a Science Research Center (Molecular Therapy Research Center) grant from the Korea Science and Engineering Foundation. The costs of publication of this article were defrayed in part by the payment of page charges. This article must therefore be hereby marked "*advertisement*" in accordance with 18 U.S.C. Section 1734 solely to indicate this fact.

[1] Both authors contributed equally to the work.

[2] To whom correspondence should be addressed. Tel.: 82-2-3410-3510; Fax: 82-2-3410-6829; E-mail: jeholee@unitel.co.kr.

[3] The abbreviations used are: TB, thymosin β; EM, energy minimization; MD, molecular dynamics; r.m.s.d., root mean square deviation(s); WT, wild type; PBS, phosphate-buffered saline; X-gal, 5-bromo-4-chloro-3-indolyl-β-D-galactopyranoside; GST, glutathione *S*-transferase; GFP, green fluorescent protein.

module in the INSIGHTII program in computer-generated three-dimensional structures. For structural and energy comparisons against wild type (WT) TB10, the 12 mutant structures were refined using the protocol described above. Because this protein consists of a small number of amino acids, it is possible that in the ground state the structure may have several or multiple stable conformations rather than one unique state. To confirm the possibility, four trials of MD simulations of each system were performed over 14 systems (12 mutants and WT TB9 and TB10).

Site-directed Mutagenesis of Human TB10—All PCR amplifications were carried out using *Pfu* DNA polymerase (Stratagene, La Jolla, CA) according to the manufacturer's recommendations. The cDNA sequence encoding human TB10 was amplified by PCR from pQBI-Ad-TB10 (21) as a template using two specific primers (forward, 5′-CGGGAATTCATGGCAGACAAACCAGAC-3′, and reverse, 5′-CCGCTCGAGTTAGGAAATTTCACTCCG-3′). The PCR product obtained was cleaved with EcoRI and XhoI and cloned into pcDNA3 expression vector (Invitrogen). All 12 point mutants of the TB10 gene were obtained using the QuikChange (Stratagene) site-directed mutagenesis kit, according to the manufacturer's instructions. The sequences of mutated residues were confirmed by automatic sequencing (ABI 373, PerkinElmer Life Sciences).

Transfection, Growth Inhibition, and Apoptosis Assays—Cancer cell lines of SKOV-3 and PA-1 were grown in Dulbecco's modified Eagle's medium (Whittaker Bioproducts, Walkersville, MD) supplemented with 10% fetal bovine serum and 1% penicillin/streptomycin at 37 °C in a 5% CO_2 atmosphere. After 24 h, SKOV-3 and PA-1 cells were transfected using FuGENE 6 (Roche Applied Science) with 5 μg of DNA in 6-well plates for 48 h. After transfection the cells were harvested, stained with trypan blue, and counted under a light microscope. To detect apoptotic cells, PA-1 and SKOV-3 ovarian cancer cell lines were also plated onto 4-chamber slides. Two days after transfection, chamber slides were rinsed with phosphate-buffered saline (PBS), stained with 2 mg/ml 4′,6-diamidino-2-phenylindole (Roche Applied Science) at 37 °C for 15 min, washed twice with PBS, and examined under a fluorescence microscope.

Fluorescence Detection of F-actin—Monolayers of SKOV-3 and PA-1 were fixed for 40 min at room temperature with 4% paraformaldehyde in PBS and then stained with phalloidin-fluorescein isothiocyanate (Sigma) (25 μg/ml) for 1 h in the dark. Stained cell monolayers were washed twice with 0.5% Triton X-100 in PBS. Coverslips were mounted onto slides using a PBS/glycine mountant and examined under a fluorescence microscope.

Yeast Two-hybrid Analysis, in Vitro Binding Assay, and Coimmunoprecipitation—The interactions between TB10 (WT or mutants) and G-actin were examined using the yeast two-hybrid system. A positive interaction was defined as an ability to support cell growth on leucine-depleted media or by a blue result by white color testing on X-gal-containing media (22). DNAs encoding human TB10 WT or T20S mutant (Thr^{20} to Ser^{20} mutation) for *in vitro* binding assay was ligated into pGEX4T-1 (Amersham Biosciences) using EcoRI and SalI to generate glutathione *S*-transferase (GST) fusion protein. DNA encoding for human G-actin was subcloned into pET29a (Novagen, Madison, WI). GST and His fusion proteins were purified according to the manufacturer's instructions. For coimmunoprecipitation, we transfected the plasmids containing pEGFPC1-G-actin and pcDNA3.1-TB10(WT) or T20S mutant into SKOV-3 cells, immunoprecipitated G-actin with the antibody to GFP, resolved by SDS-PAGE, and immunoblotted with antibodies to GFP, TB10, and actin.

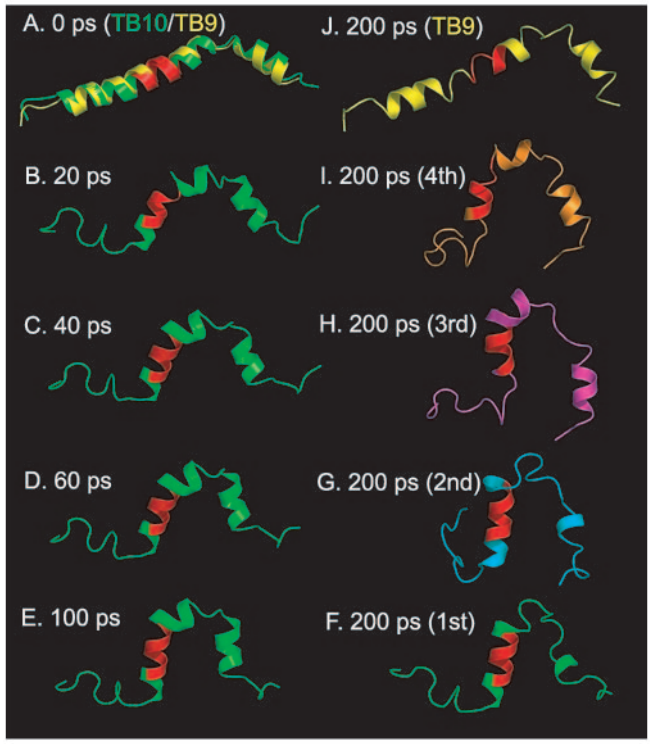

FIGURE 1. **Computer generated three-dimensional human TB10 structures with a calf thymus TB9 structure.** *A*, homology-modeled WT structure of human TB10 (*green*) is rendered as a ribbon diagram along with the template NMR structure of calf TB9 (*yellow*). *B–F*, five additional MD snapshot conformations from 200-ps MD simulations of the TB10 structure are shown in the same format to show structural changes during 200-ps simulation. *G–I*, three additional MD snapshot structures from different trajectories are displayed for comparison. *J*, final MD snapshot conformation of the 200-ps MD simulation of the TB9 structure. The location of the key motif residues, ^{17}LKKTET^{22}, is highlighted in *red* for clarity.

RESULTS AND DISCUSSION

Three-dimensional Structure of Human TB10—The dynamic equilibrium established between G- and F-actin is important during embryonic development, angiogenesis, and metastasis (23–26). Modulations of actin stability by proteins that sequester actin monomers like thymosins control these processes. Most β-thymosin family members contain the hexapeptide motif LKKTET, which is highly conserved in a number of other actin-binding proteins, *e.g.* α-actinine, villin, dematin, tropomyosin, and actobindin (27).

To consider a three-dimensional structural change in a new environment, the homologous three-dimensional structure must be refined by MD simulation. To perform MD simulations, the initial three-dimensional structure of each system was surrounded by a 10-Å water layer composed of 1413 water molecules. After the entire system had been energy-minimized using a conjugate gradient algorithm, 200-ps MD simulation was performed.

The first computer-generated three-dimensional structure of WT TB10 was aligned with the NMR-determined TB9 template, as shown in Fig. 1*A*. The secondary structure of the first version TB10 structure, which was not refined yet, was a helix-turn-helix structure, in which the turn was located at residues 30–33. Moreover, its conserved motif was located in the long helix structure. However, a 200-ps MD simulation resulted in a distinctive structural change in TB10 as compared with the original TB9 structure. The severe bend was observed in 100-ps simulations (Fig. 1, *B–E*), and they were also found in the three additional trials (Fig. 1, *G–I*). Fig. 1 shows that TB10 contains two turns in the

TABLE ONE

Potential energy comparisons for EM and MD simulations

Energy values were collected from the four trials of MD simulations. All of the values are the relative energies (ΔE) from values of WT in kcal/mol.

Name	For EM[a]	For MD[a]
WT	0.00	0.00
L17A	27.01	−43.27
K18A	−0.90	−2.06
K19A	67.08	47.70
T20A	−24.32	−28.52
E21A	190.89	165.9
T22A	−1.35	−12.12
L17S	7.48	−39.04
K18S	23.39	82.54
K19S	70.90	23.95
T20S	−24.57	−21.47
E21S	195.20	184.48
T22S	−3.19	3.41

[a] ΔE from WT.

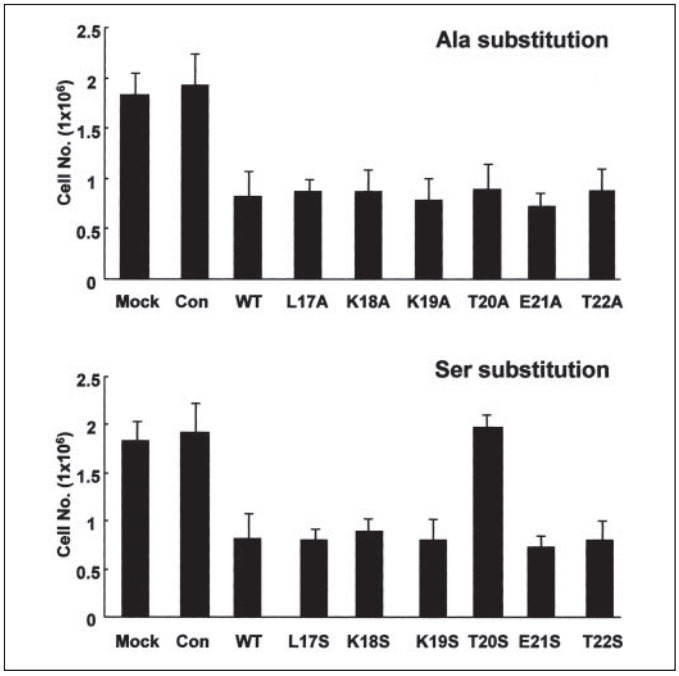

FIGURE 2. **Effect of TB10 mutants on the growth of ovarian cancer cell lines PA-1 (data not shown) and SKOV-3.** Cells were plated in 6-well dishes and transiently transfected with expression vectors encoding WT and various TB10 mutants. Cell growth was measured at 48 h, and data were obtained from three separate cultures. The results are means ± S.E. of three independent experiments. *Con*, control.

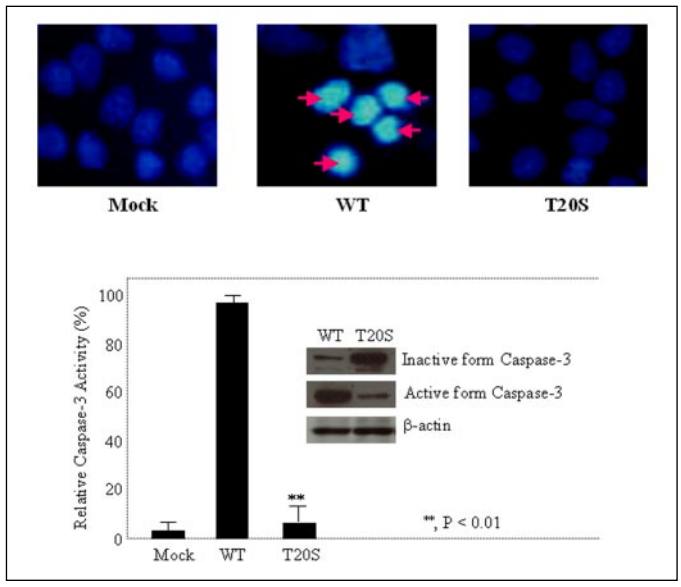

FIGURE 3. **Analysis of apoptotic cell death induced by TB10 transfection in ovarian cancer cell lines PA-1 (data not shown) and SKOV-3.** Cells were plated onto 4-chamber slides at densities of 4.5×10^4 cell/well and cultured for 1 day. Cells were stained with 4′,6-diamidino-2-phenylindole to visualize DNA fragmentation. *Arrows* indicate observed DNA fragmentations.

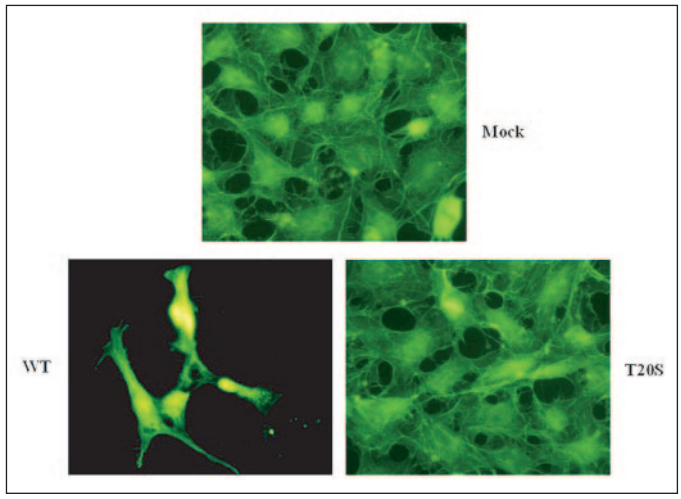

FIGURE 4. **Phalloidin-fluorescein isothiocyanate-stained F-actin.** PA-1 (data not shown) and SKOV-3 cells were transfected with WT and various mutants of TB10. Control and mock-treated cells show intact and pervasive actin stress fibers. The overexpression of WT or various mutants (data not shown) of TB10 severely disrupted the F-actin network. However, the overexpression of T20S mutant TB10 left the F-actin structure unaltered.

structure, whereas TB9 has only one. It appears that the severe bend was caused by an additional turn that is located among the 10–15 residues. The root mean square deviations (r.m.s.d.) of backbone atoms of WT TB10 between the starting and final snapshot structures were about 9 Å over the four structures. Because the four different MD simulations showed the same trend, the large bend structure seems to be the natural form of the human TB10 structure. To check whether the bend originated from the artifact of the MD simulation, the identical procedures were applied to the NMR TB9 structure. Four trials of 200-ps MD simulations of the TB9 structure showed no severe bent form (Fig. 1*J*), and moreover the final 200-ps snapshot structure was almost the same as the starting structure. The r.m.s.d. of TB9 between the starting and the final structure was less than 1.9 Å. Therefore, the bent form is believed to be a characteristic of the TB10 structure. Sequence comparisons showed that only two residues were different in the long helix region, namely, residues 6 and 10. Moreover, Leu^6 and Asp^{10} in TB9 are replaced by Met^6 and Ala^{10} in TB10. We believe that the change of Ala^{10} to Asp^{10} in the position of residue 10 explains the structural difference between TB9 and TB10, because residue 10 is located at the near of the new turn and because the size difference of the two side chains is remarkable.

Computational Mutation Experiments—Computational mutation experiments were performed to obtain information on key residues in the conserved ^{17}LKKTET^{22} motif. Six key residues in the homology-modeled three-dimensional WT structure were mutated to alanine and serine to produce 12 different mutant structures. Four 200-ps MD simulations were carried out for each of the 12 mutant structures. Final MD

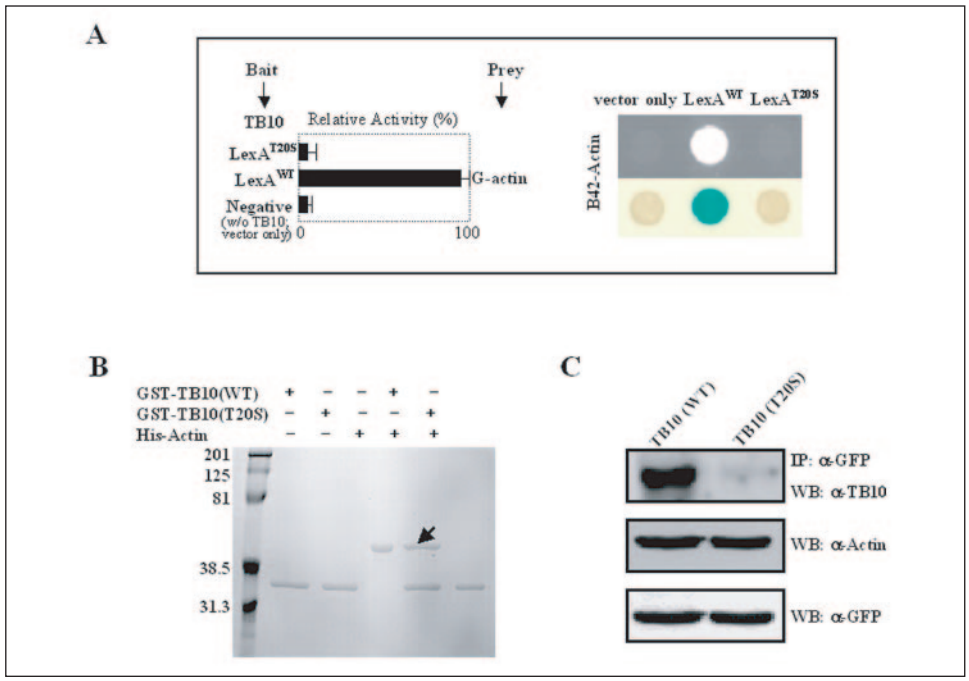

FIGURE 5. **Interaction between TB10 (WT), mutant T20S, and G-actin.** *A*, WT and the T20S mutant of human TB10 were tested with respect to their ability to interact with G-actin by using yeast two-hybrid assays. Positive interactions were determined by examining cell growth on leucine-depleted medium, and by the formation of blue colonies on medium containing X-gal or in liquid medium using *O*-nitrophenyl β-D-galactopyranoside as substrate. *B*, interactions between TB10 [GST·TB10 (WT) and T20S mutant] and G-actin (His-G-actin) were confirmed by *in vitro* binding assays. GST·TB10 (WT) and GST·TB10 (T20S) fusion proteins were mixed with His-G-actin. Mixtures were subjected to glutathione affinity purification. The co-purification of His-G-actin and GST·TB10 (WT), but not with GST·TB10 (T20S), is shown by the *arrow*. *C*, coimmunoprecipitation of pEGFPC1-G-actin and pcDNA-TB10 (WT, T20S) in SKOV-3 cells. *IP*, immunoprecipitation; *WB*, Western blotting with indicated antibodies.

snapshot structures of the 12 mutants were collected, and their structures were compared with the WT using r.m.s.d. measurements. The potential energies from the EM structures and MD snapshot structures were collected from the 12 mutant structures and then compared with those of the WT. No distinctive r.m.s.d. (or structural) change was found in any of the 12 mutant structures, and the averaged r.m.s.d. values for starting and final structures were ~9 Å. TABLE ONE shows that the potential energy of EM structures showed some remarkable features for point mutations at the positions of residues 20 and 21. It showed that the mutation of residue 20 caused remarkable energy stabilization but the mutation of residue 21 resulted in the most significant energy destabilization of the system. The same features concerning positions 20 and 21 were also shown by the potential energy results that were produced from MD structures. However, the results from the MD cases showed additional negative potential energy changes at position 17. Because these kinds of abrupt energy changes caused by the point mutation imply that the amino acid in the particular position should be conserved as the original one, we conclude that positions 20 and 21 are the two best candidates for the key residues for the protein function.

Effect of TB10 Point Mutations on Growth in Ovarian Cancer Cells—We tested the contribution made by individual amino acids in the ^{17}LKKTET^{22} motif to the biological activity of TB10 by Ala and Ser scanning mutagenesis. Each of the mutant sequences was confirmed by automatic sequencing, and transfected to SKOV-3 and PA-1 (data not shown) ovarian cancer cells. Three days after transfection, cells were harvested and stained with trypan blue, and apoptotic events were counted. As shown in Fig. 2, WT TB10-transfected cancer cells showed clear growth arrest, suggesting that overexpressed TB10 induced massive cell death. Moreover, only one of the mutants, T20S, restored cell growth.

To better understand the structural-functional relationships of the conserved ^{17}LKKTET^{22} motif, we also stained SKOV-3 and PA-1 (data not shown) ovarian cancer cells with 4′,6-diamidino-2-phenylindole to confirm that the observed loss of viability was due to apoptosis. Transfectants containing only WT TB10 showed clear DNA fragmentation, whereas mock transfectants or the transfectant containing the TB10 (T21S) mutant showed no signs of DNA fragmentation (Fig. 3). Moreover, staining with phalloidin-fluorescein isothiocyanate-labeled anti-actin antibody revealed the presence of an intact and pervasive actin structure in the control and in cells transfected with the parent vector. However, when WT TB10 and all of the mutant TB10 proteins were expressed F-actin stress fibers were dramatically disrupted, but T20S-mutated TB10 overexpression did not effect any F-actin stress fiber change (Fig. 4). This result suggests that the Thr^{20} residue is a critical amino acid that helps determinate the actin-binding structure and provides an important clue about the possible tertiary structure of TB10.

The actin-binding activity of TB4 is severely compromised by the mutation of leucine 17 to alanine (L17A) (28). The C terminus shows greatest heterogeneity among members of the β-thymosin family (29). Truncations of either 13 or 19 amino acids from the C terminus reduce the actin-binding affinity of TB4. Similarly, Huff *et al.* (30) reported that the removal of the last two C-terminal amino acids of TB10 reduces its actin-binding affinity by an ultrafiltration assay. Moreover, the centrally conserved motif ^{17}LKKTETQ^{23} of TB10 is shared by several monomeric actin-binding proteins including the β-thymosins and actobindin and has been shown to be an essential actin-binding domain (31). In this study the actin-binding affinity of TB4 was studied by ultrafiltration assay, but the activity of mutated TB4 was not studied in cells.

To explore the binding activity of this conserved motif in cells, we examined the actin-sequestering effect of mutant TB10s to identify critical residues. Accordingly, we created a three-dimensional structure of human TB10 and performed modeling studies. Based on the results obtained, we propose that the T20 position critically determines the structure of the protein. We also validated this model by transfecting site-mutated TB10 variants into ovarian cancer cell lines. With the exception of T20S, none of the mutants restored cell growth. Together with the previous ultrafiltration assay results our findings demonstrate that Thr^{20} is a critical residue that helps determine the actin-binding structure of TB10.

Interaction between TB10 (WT) and Mutant T20S with G-actin in Vivo and in Vitro—To investigate the interaction between TB10 and G-actin, we conducted yeast two-hybrid assays. Positive interactions were defined by cell growth on leucine-depleted medium and by the formation of blue colonies on medium containing X-gal or in liquid

medium using *O*-nitrophenyl β-D-galactopyranoside as substrate. These studies showed a strong interaction between WT TB10 and G-actin but no such interaction with TB10 (T20S) mutant (Fig. 5*A*). This interaction was confirmed by *in vitro* binding assays and coimmunoprecipitation. As shown in Fig. 5, *B* and *C*, cellular interaction between WT TB10 and G-actin was also evident by *in vitro* binding analyses and coimmunoprecipitation. Moreover, although WT TB10 was found to interact strongly with G-actin, no such interaction was observed between TB10 (T20S) and G-actin. These results indicate that T20S mutant TB10 cannot bind G-actin and thus cannot cause TB10-mediated ovarian cancer cell apoptosis.

Recently, Philp *et al.* (32) reported that the ^{17}LKKTETQ^{23} motif of TB4 is essentially required for endothelial cell migration by binding actin. However, they did not identify the amino acid residue in the ^{17}LKKTETQ^{23} motif required to bind actin. Herein, we demonstrate that the Thr^{20} residue is important for actin binding *in vivo* and *in vitro* and that changing the Thr^{20} residue to Ser^{20} abrogates TB10-mediated apoptosis. Thus, it will be interesting to determine whether replacing Thr^{20} with Ser^{20} also blocks endothelial cell migration.

Taken together, our study demonstrates that actin-sequestering determinants mediate the apoptosis of ovarian cancer cells and that this is related to stress fiber disruption. Moreover, our study provides a detailed understanding of the structure of TB10 and of the influence of its actin-binding region.

In summary, to identify the residues critical for TB10-mediated apoptosis, a series of computational and biochemical experiments were performed. The three-dimensional structure of human TB10 was built using a homology-modeling method with the calf TB9 NMR structure. The initial modeled structure was then refined by EM and 200-ps MD simulations, and the refined structure obtained was distinctly different from the initial structure. A computer-aided mutation experiment identified positions 17, 20, and 21 as potentially key residues in the conserved ^{17}LKKTET^{22} motif for TB10 activity. Using biochemical methods, we examined the conserved motif region by Ala and Ser scanning mutagenesis. These TB10 mutants were then transfected into ovarian cancer cell lines, and their effects on growth arrest were investigated. Of the 12 possible mutations, only the T20S mutation showed an abrogated TB10 growth arrest function. These results strongly support the notion that Thr^{20} is an essential motif for actin sequestration in ovarian cancer cells and provide information useful for the design of new cancer inhibitors.

Acknowledgments—We are grateful to Dr. S. A. Martinis (Department of Biochemistry, University of Houston) and Dr. M. Tukalo (European Molecular Biology Laboratory) for critical readings of the manuscript.

REFERENCES

1. Horecker, B. L., and Morgan, J. I. (1984) *Lymphokines* **9,** 15–35
2. Low, T. L. K., Hu, S.-K., and Goldstein, A. L. (1981) *Proc. Natl. Acad. Sci. U. S. A.* **78,** 1162–1166
3. Ruggieri, S., Erickson-Viitanen, S., and Horecker, B. L. (1983) *Arch. Biochem. Biophys.* **226,** 388–392
4. Hannappel, E., Kalbacher, H., and Voelter, W. (1988) *Arch. Biochem. Biophys.* **260,** 546–551
5. Yamamoto, M., Shoda, A., Minamino, N., Matsuo, H., Nishimatsu, S., Ueno, N., and Murakami, K. (1992) *Biochem. Biophys. Res. Commun.* **184,** 93–99
6. Huff, T., Muller, C. S., Otto, A. M., Netzker, R., and Hannappel, E. (2001) *Int. J. Biochem. Cell Biol.* **33,** 205–220
7. Yu, F. X., Lin, C. S., Morrison-Bogorad, M., Atkinson, M. A., and Yin, H. L. (1993) *J. Biol. Chem.* **268,** 502–509
8. Jean, C., Rieger, K., Blanchoin, L., Carlier, M. F., Lenfant, M., and Pantaloni, D. (1994) *J. Muscle Res. Cell Motil.* **15,** 278–286
9. Hannappel, E., and Wartenberg, F. (1993) *Biol. Chem. Hoppe-Seyler* **374,** 117–122
10. Heintz, D., Reichert, A., Mihelic, M., Voelter, W., and Faulstich, H. (1993) *FEBS Lett.* **329,** 9–12
11. Huff, T., Zerzawy, D., and Hannappel, E. (1995) *Eur. J. Biochem.* **230,** 650–657
12. Lin, S. C., and Morrison-Bogorad, M. (1990) *J. Mol. Neurosci.* **2,** 35–44
13. Carpintero, P., Franco del Amo, F., Anadon, R., and Gomez-Marquez, J. (1996) *FEBS Lett.* **394,** 103–106
14. Verghese-Nikolakaki, S., Apostolikas, N., Livaniou, E., Ithakissios, D. S., and Evangelatos, G. P. (1996) *Br. J. Cancer* **74,** 1441–1444
15. Califano, D., Monaco, C., Santelli, G., Giuliano, A., Veronese, M. L., Berlingieri, M. T. Franciscis, V., Berger, N., Trapasso, F., Santoro, M. Viglietto, G., and Fusco, A. (1998) *Cancer Res.* **58,** 823–828
16. Hall, A. K. (1995) *Cell. Mol. Biol. Res.* **41,** 167–180
17. Gutierrez-Pabello, J. A., McMurray, D. M., and Adams, L. G. (2002) *Infect. Immun.* **70,** 2121–2127
18. Stoll, R., Voelter, W., and Holak, T. A. (1997) *Biopolymers* **41,** 623–634
19. Deleted in proof
20. Dauber-Osguthorpe, P., Roberts, V. A., Osguthorpe, D. J., Wolff, J., Genest, M., and Hagler, A. T. (1988) *Proteins Struct. Funct. Genet.* **4,** 31–47
21. Lee, S. H., Zhang, W., Choi, J. J., Cho, Y. S., Oh, S. H., Kim, J. W., Hu, L., Xu, J., Liu, J., and Lee, J. H. (2001) *Oncogene* **20,** 6700–6706
22. Rho, S. B., Lee, K. H., Kim, J. W., Shiba, K., Jo, Y. J., and Kim, S. (1996) *Proc. Natl. Acad. Sci. U. S. A.* **93,** 10128–10133
23. Fidler, I. J., Gersten, D. M., and Hart, I. R. (1978) *Adv. Cancer Res.* **28,** 149–250
24. Zetter, B. R. (1990) *N. Engl. J. Med.* **332,** 605–612
25. Stossel, T. P. (1993) *Science* **260,** 1086–1094
26. Devineni, N., Minamide, L. S., Niu, M., Safer, D., Verma, R., Bamburg, J. R., and Nachmias, V. T. (1999) *Brain Res.* **823,** 129–140
27. Vancompernolle, K., Goethals, M., Huet, C., Louvard, D., and Vandekerchkhove, J. (1992) *EMBO J.* **11,** 4739–4746
28. Van Troys, M., Dewitte, D., Goethals, M., Cariler, M. F., Vandekerckhove, J., and Ampe, C. (1996) *EMBO J.* **15,** 201–210
29. Eadie, J. S., Kim, S.W., Allen, P. G., Hutchinson, L. M., Kantor, J. D., and Zetter, B. R. (2000) *J. Cell. Biochem.* **77,** 277–287
30. Huff, T., Muller, C. S., and Hannappel, E. (1997) *FEBS Lett.* **414,** 39–44
31. Vancompernolle, K., Vandekerchkhove, J., Bubb, M. R., and Korn, E. D. (1991) *J. Biol. Chem.* **266,** 15427–15431
32. Philp, D., Huff, T., Gho, Y. S., Hannappel, E., and Kleinman, H. K. (2003) *FASEB J.* **17,** 2103–2105